Mineralogical Magazine, February 2017, Vol. 81(1), pp. 123–134

Structural and compositional variations of basic Cu(II) chlorides in the herbertsmithite and gillardite structure field

MATTHEW J. SCIBERRAS[1,*], PETER LEVERETT[1], PETER A. WILLIAMS[1], JOCHEN SCHLÜTER[2], THOMAS MALCHEREK[2], MARK D. WELCH[3], PETER J. DOWNES[4], DAVID E. HIBBS[5] AND ANTHONY R. KAMPF[6]

[1] School of Science and Health, Western Sydney University, Locked Bag 1797, Penrith NSW 2751, Australia
[2] Mineralogisch-Petrographisches Institut, Universität Hamburg, Grindelallee 48, D-20146 Hamburg, Germany
[3] Mineral and Planetary Sciences Division, Department of Earth Sciences, Natural History Museum, Cromwell Road, London SW7 5BD, UK
[4] Western Australian Museum, Locked Bag 49, Welshpool DC, Western Australia 6986, Australia
[5] Faculty of Pharmacy, University of Sydney, NSW 2006, Australia
[6] Mineral Sciences Department, Natural History Museum of Los Angeles County, 900 Exposition Boulevard, Los Angeles, CA 90007, USA

[*Received 12 November 2015; Accepted 27 January 2016; Associate Editor: G. Diego Gatta*]

ABSTRACT

Natural samples of the substituted basic Cu(II) chloride series, $Cu_{4-x}M^{2+}_x(OH)_6Cl_2$ (M = Zn, Ni, or Mg) were investigated by single-crystal X-ray diffraction in order to elucidate compositional boundaries associated with paratacamite and its congeners. The compositional ranges examined are $Cu_{3.65}Zn_{0.35}(OH)_6Cl_2$ – $Cu_{3.36}Zn_{0.64}(OH)_6Cl_2$ and $Cu_{3.61}Ni_{0.39}(OH)_6Cl_2$ – $Cu_{3.13}Ni_{0.87}(OH)_6Cl_2$, along with a single Mg-bearing phase. The majority of samples studied have trigonal symmetry ($R\bar{3}m$) analogous to that of herbertsmithite (Zn) and gillardite (Ni), with $a \approx 6.8$, $c \approx 14.0$ Å. Crystallographic variations for these samples caused by composition are compared with both published and new data for the $R\bar{3}m$ sub-cell of paratacamite, paratacamite-(Mg) and paratacamite-(Ni). The observed trends suggest that the composition of end-members associated with the paratacamite congeners depend upon the nature of the substituting cation.

KEYWORDS: paratacamite, paratacamite-(Mg), paratacamite-(Ni), herbertsmithite, gillardite, compositional boundary, crystal structure.

Introduction

PARATACAMITE, $Cu_3(Cu,Zn)(OH)_6Cl_2$, trigonal, space group $R\bar{3}$ (Smith 1906; Frondel 1950; Fleet 1975; Welch *et al*., 2014), is a member of the substituted basic Cu(II) chloride group of minerals. Two newly described paratacamite congeners, paratacamite-(Ni), $Cu_3(Ni,Cu)(OH)_6Cl_2$ (Sciberras *et al*., 2013) and paratacamite-(Mg), $Cu_3(Mg,Cu)(OH)_6Cl_2$ (Kampf *et al*., 2013*a*), are characterized by extensive substitution for Cu in the interlayer sites. Jambor *et al*. (1996) reported that clinoatacamite, $Cu_2(OH)_3Cl$, monoclinic, space group $P2_1/n$, transforms structurally to a trigonal phase, assumed to be paratacamite, when 2–3 wt.% Zn or Ni occupies its structure. The associated solid-solution series is apparently continuous and extends to the minerals herbertsmithite, $Cu_3Zn(OH)_6Cl_2$ (Braithwaite *et al*., 2004), gillardite, $Cu_3Ni(OH)_6Cl_2$ (Colchester *et al*., 2007; Clissold *et al*., 2007), leverettite, $Cu_3Co(OH)_6Cl_2$ (Kampf *et al*., 2013*b*) and tondiite, $Cu_3Mg(OH)_6Cl_2$ (Malcherek *et al*., 2014) (isostructural, trigonal, space group $R\bar{3}m$), depending upon the nature of the dominant substituting cation. This $R\bar{3}m$ structure corresponds to a pronounced substructure inherent in paratacamite (Fleet, 1975; Kampf *et al*., 2013*a*; Sciberras *et al*., 2013; Welch *et al*., 2014) and may be considered as the aristotype model for the group of basic Cu(II) chlorides (Malcherek and Schlüter,

*E-mail: matthew.sciberras@gmail.com
https://doi.org/10.1180/minmag.2016.080.079

2009). This group has received much attention in recent years due to their structure-induced magnetic properties, as they are so-called 'frustrated antiferromagnets' (Schores *et al*., 2005; Helton *et al*., 2007; Freedman *et al*., 2010; Chu *et al*., 2010; Han *et al*., 2011, 2012; Li and Zhang, 2013).

Malcherek and Schlüter (2009) suggested that the sequence of compositionally related structural transformations that lead to herbertsmithite can be described by the space group chain $P\bar{1} \rightarrow P2_1/c$ $(P2_1/n) \rightarrow R\bar{3}m$. However, the triclinic phase originally attributed to the series, known as 'anatacamite', has recently been discredited by the Commission on New Minerals Nomenclature and Classification of the International Mineralogical Association (Hålenius *et al*., 2015). Welch *et al*. (2014) reported a reversible structural transformation from paratacamite $R\bar{3}$ to herbertsmithite $R\bar{3}m$ structures that occurs at 353–393 K. This transformation is in line with the predicted space group chain associated with the paratacamite phase, $P\bar{1} \rightarrow R\bar{3} \rightarrow R\bar{3}m$ (Malcherek and Schlüter, 2009). The boundary between the $R\bar{3}$ and $R\bar{3}m$ phases is difficult to quantify due to the very similar powder X-ray diffraction patterns of the minerals (Jambor *et al*., 1996; Braithwaite *et al*., 2004; Kampf *et al*., 2013*a*; Sciberras *et al*., 2013). The superstructure reflections of paratacamite may only be quantifiable using single-crystal diffraction methods (Kampf *et al*., 2013*a*; Sciberras *et al*., 2013; Welch *et al*., 2014).

Braithwaite *et al*. (2004) suggested an upper compositional limit for the stability of paratacamite of ~50% interlayer occupancy of Zn, which implies a destabilization of the herbertsmithite structure below this threshold. Paratacamite from the type material (British Museum specimen BM86958) was reported by Welch *et al*. (2014) as having the composition $Cu_{3.71}Zn_{0.29}(OH)_6Cl_2$, which is in line with the observations made by Braithwaite *et al*. (2004) and Jambor *et al*. (1996). However, recent reports of paratacamite-(Mg) (Kampf *et al*., 2013*a*) and paratacamite-(Ni) (Sciberras *et al*., 2013) both with a composition significantly >50% occupancy of the interlayer by the substituting cation has indicated that the compositional stability fields of paratacamite and herbertsmithite congeners may be significantly different from those of these two minerals.

This crystallographic investigation of naturally occurring samples from the series was carried out to elucidate the compositional boundary between the $R\bar{3}$ and $R\bar{3}m$ structures in terms of Zn and Ni substitution.

Experimental

Samples and analysis

Specimens of the basic Cu(II) chlorides were obtained from the Mineralogical Museum, Hamburg, Germany, and from several private collections for compositional and crystallographic analysis. The authors analysed samples of paratacamite from the British Museum, London, UK (specimen BM86958), paratacamite-(Mg) from the Natural History Museum of Los Angeles County, USA (specimen 64041) and paratacamite-(Ni) from the Western Australian Museum, Western Australia, Australia (specimen WAM M365.2003), in this study, but full data of the analyses appear in the separate publications Welch *et al*., (2014), Kampf *et al*. (2013*a*) and Sciberras *et al*. (2013), respectively. Additional analyses of these samples are included in this paper. The remainder of samples and their localities are reported in Table 1.

Two different electron microprobes were used, a JEOL 8600 electron microprobe for samples originating from 132N nickel mine, Widgiemooltha, Western Australia, and a Cameca SX 100 electron microprobe for the remaining samples. Both microprobes were operated in wavelength dispersive mode with an accelerating voltage of 15 kV, a specimen current of 20 nA and focused beam. Table 1 also lists the empirical formulae determined from these analyses. The simplified formula, based on Σ (cations) = 4, for each sample was used in the structural refinement and is reported as follows: CB03, $Cu_{3.61}Ni_{0.39}(OH)_6Cl_2$; CB07, $Cu_{3.51}Ni_{0.49}(OH)_6Cl_2$; G8502, $Cu_{3.12}Ni_{0.88}(OH)_6Cl_2$; G8568, $Cu_{3.11}Ni_{0.88}Co_{0.01}(OH)_6Cl_2$; G7751, $Cu_{3.09}Ni_{0.90}Co_{0.01}(OH)_6Cl_2$; MD166-3, $Cu_{3.65}Zn_{0.35}(OH)_6Cl_2$; MM02, $Cu_{3.61}Zn_{0.39}(OH)_6Cl_2$ and MD166-2, $Cu_{3.36}Zn_{0.64}(OH)_6Cl_2$.

Crystallographic measurements

Crystals of Ni-bearing specimens from the 132 N deposit G8502, G8568 and G7751, were measured at 293(2) K using a Bruker Smart 1000 CCD diffractometer with graphite-monochromated Mo*K*α radiation. The remaining samples from the Carr Boyd Rocks mine, the Murrin Murrin mine and the San Francisco mine, CB03, CB07, MM02, MD166-2 and MD166-3 were analysed at 294(2) K on a Nonius Kappa CCD diffractometer with Mo*K*α radiation. Final unit-cell dimensions were determined by a least-squares refinement of the full data sets and all structure refinements were made

https://doi.org/10.1180/minmag.2016.080.079 Published online by Cambridge University Press

https://doi.org/10.1180/minmag.2016.080.079 Published online by Cambridge University Press

TABLE 1. Electron microprobe analyses of material in this study*.

Average (above), range (below) (wt.%) Sample	Spots	CuO	ZnO	NiO	MgO	CoO	MnO	Cl	H_2O**	O≡Cl	Total	Empirical formula
CB03	100	67.29(0.93) 65.64–70.59	–	6.75(0.69) 4.54–7.70	–	–	0.01(0.02) 0–0.05	16.12(0.14) 15.78–16.42	12.59	−3.64	102.76	$(Cu_{3.63}Ni_{0.39})_{\Sigma 4.02}$ $Cl_{1.95}(OH)_{6.00}$
CB07	8	65.79(2.29) 62.99–69.65	–	8.71(1.63) 5.17–10.12	–	–	0.07(0.04) 0–0.12	16.70(0.13) 16.44–16.84	12.77	−3.77	100.27	$(Cu_{3.50}Ni_{0.49})_{\Sigma 3.99}$ $Cl_{2.00}(OH)_{6.00}$
G8502	8	60.81(0.41) 59.92–61.16	–	16.19(0.96) 14.93–17.45	0.06(0.05) 0–0.14	0.15(0.07) 0.06–0.24	–	17.23(12) 17.04–17.46	13.28	−3.89	103.83	$(Cu_{3.11}Ni_{0.88})_{\Sigma 3.99}$ $Cl_{1.98}(OH)_{6.00}$
G8568	12	60.25(1.98) 56.60–64.86	–	16.01(1.40) 13.92–18.49	0.02(0.03) 0–0.11	0.25(0.07) 0.12–0.40	–	17.40(0.26) 17.91–17.95	13.20	−3.9393	103.20	$(Cu_{3.10}Ni_{0.88}Co_{0.01})_{\Sigma 3.99}$ $Cl_{2.01}(OH)_{6.00}$
G7751	16	59.11(2.21) 55.96–62.27	–	16.32(1.33) 14.74–19.05	0.02(0.03) 0–0.10	0.24(0.10) 0.11–0.49	–	17.58(0.22) 17.24–18.00	13.10	−3.97	102.40	$(Cu_{3.07}Ni_{0.90}Co_{0.01})_{\Sigma 3.98}$ $Cl_{2.05}(OH)_{6.00}$
MD166-3	15	68.10(0.52) 67.39–69.27	6.65(0.11) 6.44–6.80	–	–	–	–	16.27(0.21) 15.98–16.85	12.63	−3.68	99.97	$(Cu_{3.67}Zn_{0.35})_{\Sigma 4.02}$ $Cl_{1.97}(OH)_{6.00}$
MM02	100	66.76(2.41) 62.03–71.94	7.32(1.67) 4.56–11.29	–	–	–	–	16.66(0.26) 16.17–17.51	12.59	−3.77	99.56	$(Cu_{3.61}Zn_{0.39})_{\Sigma 4.00}$ $Cl_{2.02}(OH)_{6.00}$
MD166-2	40	61.42(0.86) 59.96–64.91	11.93(0.83) 9.57–13.84	–	–	–	–	16.57(0.26) 16.23–17.34	12.46	−3.74	98.64	$(Cu_{3.35}Zn_{0.64})_{\Sigma 3.99}$ $Cl_{2.03}(OH)_{6.00}$

*Fields with a dash (–) represent elements not detected. **H_2O content was calculated based on 8 anions pfu.
CB03 = Carr Boyd Rocks Mine, Western Australia, Australia; CB07 = Carr Boyd Rocks Mine, Western Australia, Australia; G8502 = 132N nickel mine, Widgiemoothla, Western Australia, Australia; G8568 = 132N nickel mine, Widgiemoothla, Western Australia, Australia; G7751 = 132N nickel mine, Widgiemoothla, Western Australia, Australia; MD166-3 = San Francisco Mine, Sierra Gorda, Chile; MM02 = Murrin Murrin mine, Western Australia, Australia; MD166-2 = San Francisco Mine, Sierra Gorda, Chile.

using *SHELXL* (Sheldrick, 2008) based on atom coordinates reported for analogous phases (Braithwaite *et al*., 2004; Clissold *et al*., 2007).

Special attention was given to the identification of weak reflections at half integer positions of *h* and *k*, which correspond to the paratacamite superstructure. Pseudo-precession diffraction patterns reconstructed from the full data collections for each sample indicated the $R\bar{3}m$ substructure (Table 2), $2a^*$ superlattice reflections being absent.

Samples containing Ni as the substituting cation have unit-cell dimensions analogous to those of gillardite ($a \approx 6.8$, $c \approx 13.9$ Å). Along the compositional series studied, the *c* axis showed the greatest variation, decreasing from 13.936(2) to 13.848(2) Å as Cu is replaced by Ni. The cell dimensions of sample G7751 are $a = 6.8421(8)$ and $c = 13.848(2)$ Å, and the composition $Cu_3(Ni_{0.90}Cu_{0.09}Co_{0.01})(OH)_6Cl_2$, compare well with the unit cell reported for holotype gillardite, $a = 6.8364(1)$ and $c = 13.8459(4)$ Å, $Cu_3(Ni_{0.903}Cu_{0.081}Co_{0.012}Fe_{0.004})(OH)_6Cl_2$, by Clissold *et al*. (2007).

Similarly, Zn-bearing samples exhibited unit-cell parameters related to herbertsmithite ($a \approx 6.8$, $c \approx 14.1$ Å). The range detected expressed the varying contribution of Zn content, increasing from 14.046(9) to 14.062(4) Å, as Zn content increases. The reported unit cell for herbertsmithite is $a = 6.834$, $c = 14.075$ Å for material of end-member composition $Cu_3Zn(OH)_6Cl_2$ (Braithwaite *et al*., 2004) and is in line with the composition *vs*. unit-cell relationship determined here. These results are also in accord with the variation in cell parameters reported for synthetic trigonal Zn-bearing members of the basic Cu(II) chlorides by Jambor *et al*. (1996).

Due to the absence of any super-lattice reflections and the similarity of these unit cells with those reported for herbertsmithite and gillardite, structural refinements were made in space group $R\bar{3}m$ for all data sets. All structures were refined based on the atom coordinates established by Braithwaite *et al*. (2004) and Clissold *et al*. (2007) for herbertsmithite and gillardite, respectively, and converged to acceptable residuals and anisotropic thermal parameters. Structure refinement details can be found in Table 2. Selected crystallographic data are given in Table 3.

The paratacamite $R\bar{3}m$ sub-cell structure is an average representation of the full $R\bar{3}$ super-cell structure (Fleet 1975; Welch *et al*., 2014). Crystallographic data for the substructures of samples identified as paratacamite (BM86958) (Welch *et al*., 2014), paratacamite-(Mg) (64041) (Kampf *et al*., 2013*a*) and paratacamite-(Ni) (WAM M365.2003) (Sciberras *et al*., 2013), were refined in space group $R\bar{3}m$ after data reduction of the full set of structure factors to include only the sublattice reflections. Selected crystallographic data for the sub-cell structure of these paratacamite samples is given in Table 3.

Description of the structures

The $R\bar{3}m$ structure is characterized by layers of (4+2) Jahn-Teller distorted octahedra of composition $[CuCl_2(OH)_4]$ (centred at the *M*(2) site), which are linked together in the interlayer *M*(1) site by an $M^{2+}O_6$ octahedron. This interlayer metal position is bonded to six symmetry equivalent O atoms and exhibits a slight angular distortion. While the *M*(2) site is completely composed of Cu^{2+}, the *M*(1) site bears the extent of Cu substitution by other divalent cations with similar ionic radius. This is the same scheme of metal distribution adopted for the related $R\bar{3}m$ phases herbertsmithite (Braithwaite *et al*., 2004), gillardite (Clissold *et al*., 2007), leverettite (Kampf *et al*., 2013*b*) and tondiite (Malcherek *et al*., 2014). The $R\bar{3}$ structure of paratacamite, published in full in Welch *et al*. (2014), Kampf *et al*. (2013*a*) and Sciberras *et al*. (2013), is composed of similar layers of $[CuCl_2(OH)_4]$ (*M*(3) and *M*(4) sites), which also exhibit typical (4+2) Jahn-Teller distortion. The interlayer is composed of two metal positions (*M*(1) and *M*(2) sites), which link the sheets together via common O atoms. The *M*(1) site is octahedrally coordinated to six symmetry equivalent O atoms, similar to the $M(1)O_6$ octahedron of the $R\bar{3}m$ structure. The *M*(2) site is bonded to three symmetry equivalent O atoms (*trans*), in an apparent (2+2+2) Jahn-Teller distorted octahedron. Similarly, the interlayer metal positions of the $R\bar{3}$ structure were assigned the full extent of Cu substitution.

Results and discussion

The compositional range determined for Zn- and Ni-bearing single-crystals,

$$Cu_{3.65}Zn_{0.35}(OH)_6Cl_2 - Cu_{3.36}Zn_{0.34}(OH)_6Cl_2$$

and $Cu_{3.61}Ni_{0.39}(OH)_6Cl_2 - Cu_{3.13}Ni_{0.87}(OH)_6Cl_2$, respectively, indicates that the $R3m$ structure can exist down to the monoclinic – trigonal transition zone determined by Jambor *et al*. (1996), between *c*. $Cu_{3.75}Zn_{0.25}(OH)_6Cl_2$ to $Cu_{3.66}Zn_{0.34}(OH)_6Cl_2$. Schores *et al*. (2005) reported X-ray structural data

https://doi.org/10.1180/minmag.2016.080.079 Published online by Cambridge University Press

TABLE 2. Crystal data and structure refinements of samples in this study.

Sample	MD166-3	MM02	MD166-2	CB03
Normalized formula[a]	$Cu_{3.65}Zn_{0.35}Cl_2O_6H_6$	$Cu_{3.61}Zn_{0.39}Cl_2O_6H_6$	$Cu_{3.36}Zn_{0.64}Cl_2O_6H_6$	$Cu_{3.61}Ni_{0.39}Cl_2O_6H_6$
Formula weight	427.75	427.82	428.28	425.24
Temperature (K)	294(2)	294(2)	294(2)	294(2)
Wavelength (Å)	0.71073	0.71073	0.71073	0.71073
Crystal system	trigonal	trigonal	trigonal	trigonal
Space group	$R\bar{3}m$	$R\bar{3}m$	$R\bar{3}m$	$R\bar{3}m$
Unit-cell dimensions a(Å),	6.835(4)	6.839(7)	6.8347(9)	6.8376(8)
c (Å)	14.046(9)	14.052(4)	14.062(4)	13.936(2)
Volume (Å^3)	568.3(6)	569.2(8)	568.87(19)	564.27(11)
Z, Calculated density (g cm^{-3})	3, 3.750	3, 3.744	3, 3.750	3, 3.754
Absorption coefficient (mm^{-1})	11.885	11.880	11.976	11.717
F(000)	613	613	614	611
Crystal size (mm)	0.11×0.09×0.08	0.24×0.20×0.16	0.25×0.20×0.15	0.22×0.18×0.15
Theta range for data	3.74 to 34.98°	3.73 to 34.95°	3.73 to 34.98°	3.74 to 34.97°
Limiting indices	$-10 \le h \le 10$	$-10 \le h \le 10$	$-10 \le h \le 9$	$-10 \le h \le 10$
	$-11 \le k \le 11$	$-10 \le k \le 10$	$-10 \le k \le 11$	$-10 \le k \le 10$
	$-21 \le l \le 22$	$-22 \le l \le 22$	$-22 \le l \le 22$	$-22 \le l \le 22$
Reflections/unique	3714/339	4024/340	3797/340	8365/336
R_{int}	0.0369	0.0290	0.0289	0.0343
Completeness to theta	34.98° 99.7%	34.95° 100.0%	34.97° 100.0%	34.97° 99.7%
Refinement method	Full-matrix least-squares on F^2	Full-matrix least-squares on F^2	Full-matrix least-squares on F^2	Full-matrix least-squares on F^2
Data/restraints/parameters	339/1/18	340/1/19	340/1/19	336/1/18
Goodness-of-fit on F^2	1.326	1.322	1.415	1.279
Final R indices[I>2σ(I)] R_1, wR_2	0.0153, 0.0337	0.0191, 0.0491	0.0192, 0.0466	0.0159, 0.0385
R indices (all data) R_1, wR_2	0.0172, 0.0340	0.0204, 0.0495	0.0197, 0.0469	0.0166, 0.0387
$\Delta\rho_{max}$, $\Delta\rho_{min}$ (e.Å^{-3})	0.818 and –0.636	0.555 and –0.525	0.495 and –1.274	0.558 and –0.759

TABLE 2. (*contd.*)

Sample	CB07	G8502	G8568	G7751
Normalized formula[a]	$Cu_{3.51}Ni_{0.49}Cl_2O_6H_6$	$Cu_{3.12}Ni_{0.88}Cl_2O_6H_6$	$Cu_{3.11}Ni_{0.88}Co_{0.01}Cl_2O_6H_6$	$Cu_{3.09}Ni_{0.90}Co_{0.01}Cl_2O_6H_6$
Formula weight	424.74	422.91	422.81	422.71
Temperature (K)	294(2)	293(2)	293(2)	293(2)
Wavelength (Å)	0.71073	0.71073	0.71073	0.71073
Crystal system	trigonal	trigonal	trigonal	trigonal
Space group	$R\bar{3}m$	$R\bar{3}m$	$R\bar{3}m$	$R\bar{3}m$
Unit-cell dimensions a (Å)	6.841(4)	6.8403(8)	6.8407(9)	6.8421(8)
c (Å)	13.944(5)	13.852(2)	13.846(2)	13.848(2)
Volume (Å^3)	565.1(5)	561.30(12)	561.10(17)	561.42(11)
Z, Calculated density (g cm^{-3})	3, 3.744	3, 3.753	3, 3.754	3, 3.751
Absorption coefficient (mm^{-1})	11.666	11.622	11.616	11.603
F(000)	611	609	609	609
Crystal size (mm)	0.15×0.11×0.08	0.18×0.20×0.20	0.08×0.10×0.10	0.10×0.10×0.14
Theta range for data	3.74 to 34.99 °	3.74 to 28.16°	3.74 to 28.23°	3.74 to 28.27°
Limiting indices	$-10 \le h \le 11$	$-9 \le h \le 8$	$-8 \le h \le 8$	$-8 \le h \le 9$
	$-11 \le k \le 11$	$-8 \le k \le 8$	$-8 \le k \le 8$	$-8 \le k \le 7$
	$-22 \le l \le 21$	$-17 \le l \le 17$	$-15 \le l \le 17$	$-18 \le l \le 18$
Reflections/unique	3755/338	1462/186	1481/187	1450/189
R_{int}	0.0290	0.0254	0.0202	0.0218
Completeness to theta	34.99° 100.0%	28.16° 96.9%	28.23° 96.4%	28.27° 95.9%
Refinement method	Full-matrix least-squares on F^2	Full-matrix least-squares on F^2	Full-matrix least-squares on F^2	Full-matrix least-squares on F^2
Data/restraints/parameters	338/1/19	186/1/19	187/1/19	189/1/19
Goodness-of-fit on F^2	1.221	1.394	1.325	1.290
Final R indices [$I>2\sigma(I)$] R_1, wR_2	0.0139, 0.0327	0.0297, 0.0786	0.0221, 0.0569	0.0231, 0.0568
R indices (all data) R_1, wR_2	0.0151, 0.0330	0.0297, 0.0786	0.0222, 0.0570	0.0234, 0.0571
$\Delta\rho_{max}$, $\Delta\rho_{min}$ (e.Å^{-3})	0.444 and –0.611	0.609 and –2.449	0.467 and –1.741	0.576 and –1.5810

[a]The normalized formula used in the structure refinements was made to $\sum$(cations) = 4.

TABLE 3. Unit-cell data and selected bond lengths, distances and angles of the paratacamite substructure in space group $R\bar{3}m$.

	Interlayer	Unit-cell parameters	$M(1)$–O	O–$M(1)$–O	$M(2)$–O	$M(2)$–Cl	O–$M(2)$–O	O–$M(2)$–Cl	O···Cl		
Sample	cations	$M(x)$	a(Å)	c(Å)	(Å)	*cis* (°)	(Å)	(Å)	*cis* (°)	*cis* (°)	(Å)
[1]Paratacamite*	Cu > Zn[#]	(–)	6.827(5)	14.041(6)	2.11	(–)	1.98	2.78	(–)	(–)	3.07
[2]BM86958*	Cu > Zn	0.29	6.8247(1)	14.0298(4)	2.102(2)	103.99(7)	1.9774(9)	2.7774(6)	98.25(11)	97.59(7)	3.072(1)
[3]MD166-3	Cu > Zn	0.35	6.835(4)	14.046(9)	2.112(2)	103.77(7)	1.982(1)	2.778(1)	97.77(8)	97.59(5)	3.073(2)
[3]MM02	Cu > Zn	0.39	6.839(7)	14.052(4)	2.109(2)	103.78(6)	1.983(2)	2.781(2)	97.94(9)	97.56(5)	3.074(2)
[3]MD166-2	Zn > Cu	0.64	6.8347(9)	14.062(4)	2.114(1)	103.67(5)	1.9838(6)	2.7778(6)	97.62(7)	97.49(3)	3.072(1)
[4]Herbertsmithite	Zn > Cu	1	6.834(1)	14.075(2)	2.119(1)	(–)	1.985(1)	2.779(1)	(–)	(–)	3.071
[3]CB03	Cu > Ni	0.39	6.8376(6)	13.936(2)	2.088(1)	103.31(5)	1.9827(6)	2.7735(5)	98.42(8)	97.66(3)	3.060(1)
[3]CB07	Cu > Ni	0.49	6.841(4)	13.944(5)	2.089(1)	103.36(5)	1.983(1)	2.775(1)	98.46(7)	97.69(4)	3.063(2)
[5]Paratacamite-(Ni)*	Ni > Cu[§]	0.73	6.843(1)	13.935(3)	2.088(2)	103.39(9)	1.982(1)	2.775(8)	98.48(13)	97.75(5)	3.064(2)
[3]G8502	Ni > Cu	0.88	6.8403(8)	13.852(2)	2.077(3)	102.93(14)	1.983(2)	2.768(1)	98.48(19)	97.80(8)	3.051(3)
[3]G8568	Ni > Cu[§]	0.89	6.8407(9)	13.846(2)	2.079(2)	102.99(10)	1.981(1)	2.7673(9)	98.43(14)	97.89(6)	3.053(2)
[3]G7751	Ni > Cu[§]	0.91	6.8421(8)	13.848(2)	2.077(2)	102.94(10)	1.983(1)	2.7676(9)	98.53(14)	97.85(6)	3.053(2)
[6]Gillardite	Ni > Cu[φ]	0.90	6.8364(1)	13.8459(4)	2.0791(8)	102.93(3)	1.9812(4)	2.7665(3)	98.34(5)	97.81(2)	3.049(8)
[7]Paratacamite-(Mg)*	Mg > Cu	0.60	6.8441(8)	14.025(1)	2.104(3)	103.33(10)	1.988(1)	2.7764(9)	97.96(15)	97.49(6)	3.069(2)
[8]Tondiite	Mg > Cu	0.70	6.8345(2)	14.0022(7)	2.0971(7)	103.33(6)	1.9855(6)	2.7716(4)	98.15(6)	97.49(5)	3.0659(8)
[9]Leverettite	Co > Cu[¥]	0.67	6.8436(6)	14.064(1)	2.114(3)	103.92(11)	1.983(1)	2.782(1)	97.87(17)	97.67(7)	3.079(2)

The composition (x) corresponds to the formula $Cu_{4-x}M_x(OH)_6Cl_2$; (–) not given. [1]Average distances with respect to split sites in space group $R\bar{3}m$ of the paratacamite substructure from Fleet (1975); [2]paratacamite from the type specimen at 300 K examined in Welch *et al.* (2014); [3]this study; [4]Braithwaite *et al.* (2004); [5]Sciberras *et al.* (2013); [6]Clissold *et al.* (2007); [7]Kampf *et al.* (2013*a*); [8]Malcherek *et al.* (2014); [9]Kampf *et al.* (2013*b*). [#]True composition must be considered unknown. [¥]Also contains a small amount of Mn and trace Ni and Mg. [§]Also contains trace Co. [φ]Contains minor Co and trace Fe. *$R\bar{3}$ super-structure is considered to be the true structure.

for synthetic single-crystals of Zn-bearing paratacamite, produced by hydrothermal methods. Although, all structure refinements by these authors were made on the $R\bar{3}m$ sub-cell, the authors did not mention the presence of any super-lattice reflections and their data are in complete agreement with those for herbertsmithite. The range of compositions studied by these authors is $Cu_{3.67}Zn_{0.33}(OH)_6Cl_2$ – $Cu_3Zn(OH)_6Cl_2$, and supports these observations.

It is important to note that the $R\bar{3}m$ structure shared by herbertsmithite, gillardite, leverettite and tondiite, is topologically, but not crystallographically, identical to that of paratacamite ($R\bar{3}$) and its congeners. The former minerals, *sensu stricto*, are defined as having an interlayer site that is dominated by Zn, Ni, Co or Mg respectively (Braithwaite *et al*., 2004; Clissold *et al*., 2007; Kampf *et al*., 2013*b*; Malcherek *et al*., 2014). Guidelines for nomenclature of topologically identical phases defer to the 'dominant-constituent rule' (Hatert and Burke, 2008). Therefore, those samples exhibiting the $R\bar{3}m$ structure but with Cu dominance in the interlayer, represent a separate species that deserves a unique name. This issue will be addressed in a future manuscript.

An examination of selected crystallographic data (Table 3) for samples containing Zn^{2+} as the primary substituting cation shows that *a* and *c* axes decrease towards the monoclinic–trigonal transformation boundary, in line with the observations of powdered material in Jambor *et al*. (1996). There is a small contraction of *M*–O bond lengths for both metal sites with decreasing Zn content. All *cis*∠O–*M*–O show a corresponding increase along the series, of which the most pronounced increase is associated with the $M(1)O_6$ octahedron. The trends are generally reversed when Ni^{2+} is the dominant substituting cation. The *c* axis length increases by ~0.1 Å with decreasing Ni content. Along the same compositional trend *cis*∠O–*M*–O of both *M*(1)- and *M*(2)-centred octahedra gradually increase, with the most pronounced change existing in the *cis*∠O–*M*(1)–O.

For Zn-bearing samples, there is no significant change in the O···Cl distance with changes in composition. The Ni-bearing samples show only a minor decrease in the O···Cl distance with increasing Ni-content. Data from the paratacamite $R\bar{3}m$ structure are generally consistent with trends observed for herbertsmithite and gillardite ($R\bar{3}m$) samples.

There is no significant difference between the paratacamite-(Mg) sub-cell structure and tondiite, which only differ in composition by a small amount, where *x*(Mg) = 0.60 in paratacamite-(Mg) (Kampf *et al*., 2013*a*) and *x*(Mg) = ≈0.70 in tondiite (Malcherek *et al*., 2014) for the formula $Cu_{4-x}Mg_x(OH)_6Cl_2$. The average sub-cell structure of paratacamite-(Mg) appears consistent with variation attributed to the difference in ionic radius of the cations. The effective ionic radius of $^{[6]}Mg^{2+}$ (0.72 Å) is only marginally less than that of $^{[6]}Cu^{2+}$ and $^{[6]}Zn^{2+}$ (0.73 Å and 0.74 Å, respectively), but is larger than $^{[6]}Ni^{2+}$ (0.69 Å) (Shannon, 1976). The leverettite (Co end-member) sample has a relatively large unit cell which would be influenced to some degree by the presence of $^{[6]}Mn^{2+}$ (0.83 Å) which is significantly larger than $^{[6]}Co^{2+}$ (0.745 Å), in a six-coordinate environment (Shannon, 1976).

The lattice strain induced by composition was calculated by determining the corresponding strain tensor of the aristotype unit cell as well as the transformed paratacamite sub-cell for samples listed in Table 3. The strain tensors were then used to calculate the scalar strain. According to the crystallographic data in Table 3, the paratacamite substructure offers a good comparison with samples exhibiting the aristotype structure (*sensu stricto*). Therefore, the corresponding unit-cell strain observed for this substructure should also be comparable with the compositional trends observed for the aristotype structure. The tensor components for the hexagonal setting can be determined from the following equations:

$$e_{11} = e_{22} = \frac{a}{a_o} - 1 \quad (1)$$

$$e_{33} = \frac{C}{C_o} - 1 \quad (2)$$

$$e_{23} = e_{13} = e_{12} = 0 \quad (3)$$

The above equations are from Carpenter *et al*. (1998) and are discussed in the context of this mineral series by Malcherek and Schlüter (2009). The unit cell reported by Braithwaite *et al*. (2004) for herbertsmithite was used for reference values in the calculation giving $a_o = 6.834$ and $c_o = 14.075$ Å. The reference unit cell for gillardite, $a_o = 6.8364$ and $c_o = 13.8459$ Å, was taken from Clissold *et al*. (2007) for material of composition $(Cu_{3.081}Ni_{0.903}Co_{0.012}Fe_{0.004})(OH)_6Cl_2$. This material is not ideal as a reference for the lattice parameters expected for pure $Cu_3Ni(OH)_6Cl_2$, but was retained here because it exhibits the smallest lattice volume and highest substitution of the available gillardites in the literature of this study.

https://doi.org/10.1180/minmag.2016.080.079 Published online by Cambridge University Press

TABLE 4. Scalar strain and strain tensor components for the aristotype unit-cell.

Sample	$Zn_x^{\#}$	e_{11}	e_{22}	e_{33}	$\sqrt{\sum_{ij}^{e} 2}$
Paratacamite*	(–)	–0.0010	–0.0010	–0.0024	0.0028
BM86958*	0.29	–0.0014	–0.0014	–0.0032	0.0037
MD166-3	0.35	0.0001	0.0001	–0.0021	0.0021
MM02	0.39	0.0007	0.0007	–0.0016	0.0019
MD166-2	0.64	0.0001	0.0001	–0.0009	0.0009
Sample	$Ni_x^{\#}$	e_{11}	e_{22}	e_{33}	$\sqrt{\sum_{ij}^{e} 2}$
CB03	0.39	0.0002	0.0002	0.0065	0.0065
CB07	0.49	0.0007	0.0007	0.0071	0.0071
[5]Paratacamite-(Ni)*	0.71	0.0010	0.0010	0.0064	0.0066
G8502	0.88	0.0006	0.0006	0.0004	0.0009
G8568	0.89	0.0006	0.0006	0.0	0.0009
G7751	0.91	0.0008	0.0008	0.0002	0.0012

*The true unit-cell is the paratacamite super-cell. #The composition relates to the formula $Cu_{4-x}M_x(OH)_6Cl_2$.

Calculations were made using the unit-cell parameters in Table 3 for all Zn- and Ni-bearing samples. The trace amount of Co present in some of the gillardite samples is not expected to contribute significantly to the unit cell volume. The scalar strain and calculated tensor components can be found in Table 4 in the final column.

The distortion of the aristotype unit cell increases towards the trigonal→monoclinic transformation as the critical interlayer Cu content is approached. The

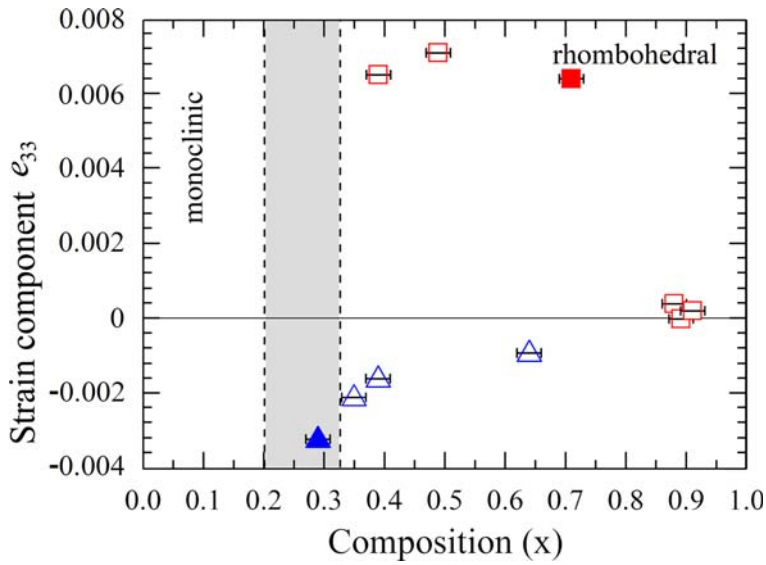

FIG. 1. The paratacamite sub-cell strain tensor e_{33} of samples used in this study. The composition x applies to the formula $Cu_{4-x}M_x(OH)_6Cl_2$ where M = Zn (blue triangles) or Ni (red squares). Filled markers are samples of the paratacamite congeners and open markers are either herbertsmithite, gillardite or their Cu-rich congeners. The dotted lines mark the proposed compositional transformation zone between monoclinic and trigonal members determined by Jambor *et al.* (1996).

https://doi.org/10.1180/minmag.2016.080.079 Published online by Cambridge University Press

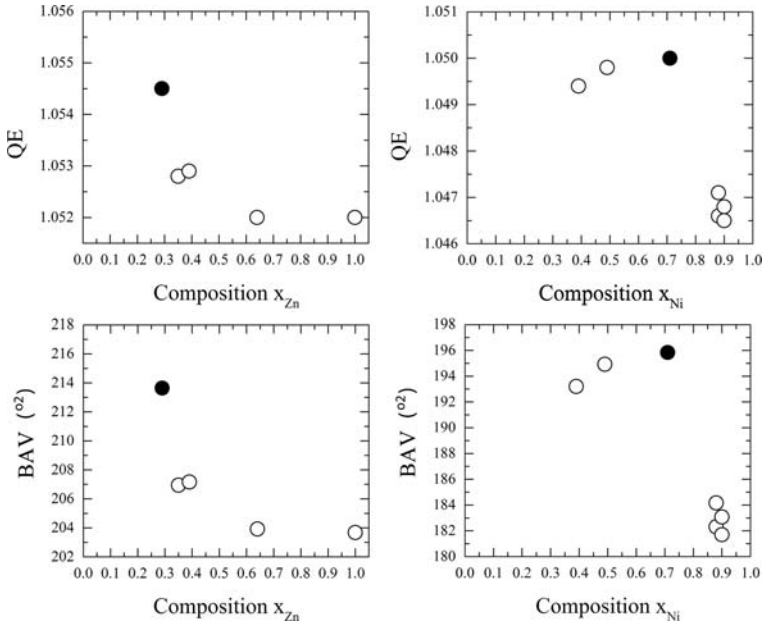

FIG. 2. Quadratic elongation (QE) and bond-angle variance (BAV) of *M*(1) interlayer octahedron of herbertsmithite, gillardite and their Cu-rich congerns (open shapes) and in the paratacamite $R\bar{3}m$ substructure (filled shapes). Compositional error bars are smaller than the size of the symbol.

strain for both chemical systems is small across the entire series, but increases much more rapidly for Ni-bearing samples. This might be due to the greater difference in ionic radius between $^{[6]}Cu^{2+}$ and $^{[6]}Ni^{2+}$, versus $^{[6]}Zn^{2+}$. The strain tensor e_{33} plot against composition is displayed in Fig. 1. The sub-cell of paratacamite (BM86958) shows the greatest strain of all Zn-bearing samples. The upper compositional limit proposed for the stability of clinoatacamite, at $x \approx 0.33$, appears to be a critical composition in terms of the aristotype unit-cell strain. Extrapolation of the trend for Zn-bearing samples indicates that the Zn composition of holotype paratacamite examined by Fleet (1975), with a scalar strain of 0.0028 associated with the sub-cell, is between *c.* $Cu_{3.70}Zn_{0.30}(OH)_6Cl_2$ and $Cu_{3.67}Zn_{0.33}(OH)_6Cl_2$.

The distortion of the *M*(1) octahedron in the $R\bar{3}m$ aristotype structure was calculated for Zn- and Ni-bearing material in this study using the formulation for quadratic elongation (QE) and bond-angle variance (BAV) of Robinson *et al.* (1971), as implemented in the program *VESTA* (Momma and Izumi, 2008). The data are displayed in Fig. 2. Both the QE and BAV values for herbertsmithite and gillardite samples show significant changes that can be related to composition. The single representative QE and BAV value determined from the paratacamite (BM86958) $R\bar{3}m$ structure, with a composition of $Cu_{3.71}Zn_{0.29}(OH)_6Cl_2$ (Welch *et al.*, 2014), has the highest distortion of all Zn-bearing samples. With increasing Zn content, both QE and BAV values decrease to a minimum for compositions above $x \approx 0.6$ and are unaffected by increased Zn content. Similarly, gillardite samples show a significant and reproducible decrease for both QE and BAV values with excess Ni content. However, the decrease in these values appears to be sharper and occurs at a composition $x > 0.7$. The $R\bar{3}m$ structure of paratacamite-(Ni) gives comparable QE and BAV values with samples having lower Ni contents.

The holotype paratacamite of Fleet (1975) has QE and BAV values associated with the interlayer octahedron of the average sub-cell structure of 1.053 and 207.64 deg^2, respectively. Extrapolation of the trends in Fig. 2 indicate a compositional range in agreement with that suggested from the scalar strain results described above.

Conclusions

The difference in trend evolution of QE and BAV values between the Zn- or Ni-bearing aristotype

https://doi.org/10.1180/minmag.2016.080.079 Published online by Cambridge University Press

structure may be attributed to the difference in crystal-chemical behaviour of these cations. These results show that the distortion exhibited by the $M(1)O_6$ octahedron varies with changes in composition in the aristotype structure. It may be inferred that the analogous interlayer position in the paratacamite superstructure at $M(1)$, which is invariant with temperature (Welch *et al*., 2014), varies with composition. Therefore, it is likely that the Zn- and Ni-bearing samples of paratacamite would have a different set of end-members. This could also be true of other paratacamite congeners. However, the end-members associated with Zn or Ni substitution in paratacamite could not be identified from this study.

Both paratacamite-(Ni) and paratacamite-(Mg) examined here have >50% interlayer occupancy of the substituting cation. This may indicate that the $R\bar{3}$ super-cell may also exist across much of the substitution series. One must consider also the multitude of structural refinements for the $R\bar{3}m$ aristotype structure with end-member or near end-member stoichiometry from the literature (Clissold *et al*., 2007; Braithwaite *et al*., 2004; Chu *et al*., 2010, 2011; Han *et al*., 2011; Chu, 2011; Wulferding *et al*., 2010; Schores *et al*., 2005). The aristotype structure appears to be thermodynamically stable near the end-member composition $Cu_3M(OH)_6Cl_2$. As the presence of Cu^{2+} becomes significant in the interlayer the $R\bar{3}$ structure may become metastable. Based on the quantifiable distortion of the interlayer position in the aristotype structure, the substituting cation defines the range of stability (or metastability) for the phase. This implies that under the right conditions paratacamite congeners would crystallize before their corresponding aristotype phase, herbertsmithite or gillardite for Zn and Ni, respectively, and by extension tondiite and leverettite for Mg and Co, respectively, described by the Ostwald step rule (Ostwald, 1897). The particular conditions which promote the nucleation and growth of the aristotype structure may serve to inhibit the nucleation and growth of $R\bar{3}$ domains.

Acknowledgements

The author MJS acknowledges financial support from the Western Sydney University for a postgraduate studies grant and a scholarship from the Deutscher Akademischer Austausch Dienst (DAAD) in the program Research Grant for Doctoral Candidates and Young Academics and Scientists A/11/93939.

References

Braithwaite, R.S.W., Mereiter, K., Paar, W.H. and Clark, A.M. (2004) Herbertsmithite, $Cu_3Zn(OH)_6Cl_2$, a new species, and the definition of paratacamite. *Mineralogical Magazine*, **68**, 527–539.

Carpenter, M.A., Salje, E.K.H. and Graeme-Barber, A. (1998) Spontaneous strain as a determinant of thermodynamic properties for phase transitions in minerals. *European Journal of Mineralogy*, **10**, 621–691.

Chu, S. (2011) Magnetic properties of geometrically frustrated polymorphic crystals of $Cu_{4-x}Mg_x(OH)_6Cl_2$. *Journal of Physics: Conference Series*, **273**, 012123.

Chu, S., McQueen, T.M., Chisnell, R., Freedman, D.E., Müller, P., Lee, Y.S. and Nocera, D.G. (2010) A Cu^{2+} ($S = ½$) kagomé antiferromagnet: $Mg_xCu_{4-x}(OH)_6Cl_2$. *Journal of the American Chemical Society*, **132**, 5570–5571.

Chu, S., Müller, P., Nocera, D.G. and Lee, Y.S. (2011) Hydrothermal growth of single crystals of the quantum magnets: clinoatacamite, paratacamite and herbertsmithite. *Applied Physics Letters,* **98,** 092508.

Clissold, M.E., Leverett, P. and Williams, P.A. (2007) The structure of gillardite, the Ni-analogue of herbertsmithite, from Widgiemooltha, Western Australia. *The Canadian Mineralogist*, **45**, 317–320.

Colchester, D.M., Leverett, P., Clissold, M.E., Williams, P. A., Hibbs, D.E. and Nickel, E.H. (2007) Gillardite, $Cu_3NiCl_2(OH)_6$, a new mineral from the 132 North deposit, Widgiemooltha, Western Australia. *Australian Journal of Mineralogy*, **13**, 15–18.

Fleet, M.E. (1975) The crystal structure of paratacamite, $Cu_2(OH)_3Cl$. *Acta Crystallographica*, **B31**, 183–187.

Freedman, D.E., Han, T.H., Prodi, A., Müller, P., Huang, Q.-Z., Chen, Y.-S., Webb, S.M., Lee, Y.S., McQueen, T.M. and Nocera, D.G. (2010) Site specific X-ray anomalous dispersion of the geometrically frustrated kagomé magnet, herbertsmithite, $ZnCu_3(OH)_6Cl_2$. *Journal of the American Chemical Society*, **132**, 16185–16190.

Frondel, C. (1950) On paratacamite and some related copper chlorides. *Mineralogical Magazine*, **29**, 34–45.

Hålenius, U., Hatert, F., Pasero, M. and Mills, S.J. (2015) New minerals and nomenclature modifications approved in 2015. *Mineralogical Magazine*, **79**, 941–947.

Han, T.H., Helton, J.S., Chu, S., Nocera, D.G., Rodriguez-Rivera, J.A., Broholm, C. and Lee, Y.S. (2012) Fractionalized excitations in the spin-liquid state of a kagomé-lattice antiferromagnet. *Nature*, **492**, 406–410.

Han, T.H., Helton, J.S., Chu, S., Prodi, A., Singh, D.K., Mazzoli, C., Müller, P., Nocera, D.G. and Lee, Y.S. (2011) Synthesis and characterisation of single crystals of the spin-½ kagome-lattice antiferromagnets $Zn_xCu_{4-x}(OH)_6Cl_2$. *Physical Review B,* **83,** 100402.

https://doi.org/10.1180/minmag.2016.080.079 Published online by Cambridge University Press

Hatert, F. and Burke, E.A.J. (2008) The IMA–CNMNC dominant-constituent rule revisited and extended. *The Canadian Mineralogist*, **46**, 717–728.

Helton, J.S., Matan, K., Shores, M.P., Nytko, E.A., Bartlett, B.M., Yoshida, Y., Takano, Y., Qiu, Y., Chung, J-H., Nocera, D.G. and Lee, Y.S. (2007) Spin dynamics of the spin-½ kagome lattice antiferromagnet $ZnCu_3(OH)_6Cl_2$. *Physical Review Letters*, **98**, 107204–107208.

Jambor, J.L., Dutrizac, J.E., Roberts, A.C., Grice, J.D. and Szymański, J.T. (1996) Clinoatacamite, a new polymorph of $Cu_2(OH)_3Cl$, and its relationship to paratacamite and "anarakite". *The Canadian Mineralogist*, **34**, 61–72.

Kampf, A.R., Sciberras, M.J., Leverett, P., Williams, P.A., Malcherek, T., Schlüter, J., Welch, M. and Dini, M. (2013*a*) Paratacamite-(Mg), $Cu_3(Mg,Cu)Cl_2(OH)_6$; a new substituted basic copper chloride mineral from Camerones, Chile. *Mineralogical Magazine*, **77**, 3113–3124.

Kampf, A.R., Sciberras, M.J., Williams, P.A. and Dini, M. (2013*b*) Leverettite from the Torrecillas mine, Iquique Provence, Chile: the Co-analogue of herbertsmithite. *Mineralogical Magazine*, **77**, 3047–3054.

Li, Y.S. and Zhang, Q.M. (2013) Structure and magnetism of S = ½ kagome antiferromagnets $NiCu_3(OH)_6Cl_2$ and $CoCu_3(OH)_6Cl_2$. *Journal of Physics: Condensed Matter,* **25,** 026003.

Malcherek, T. and Schlüter, J. (2009) Structures of the pseudo-trigonal polymorphs of $Cu_2(OH)_3Cl$. *Acta Crystallographica*, **B65**, 334–341.

Malcherek, T., Bindi, L., Dini, M., Ghiara, M.R., Molina Donoso, A., Nestola, F., Rossi, M. and Schlüter, J. (2014) Tondiite, $Cu_3Mg(OH)_6Cl_2$, the Mg-analogue of herbertsmithite. *Mineralogical Magazine*, **78**, 583–590.

Momma, K. and Izumi, F. (2008) VESTA: a three-dimensional visualization system for electronic and structural analysis. *Journal of Applied Crystallography*, **41**, 653–658.

Ostwald, W.Z. (1897) Studien über die Bildung und Umwaldung fester Korper. *1. Abhandlung: Übersattigung und Überkaltung. Zeitschrift für Physikalische Chemie*, **22**, 289–330.

Robinson, K., Gibbs, G.V. and Ribbe, P.H. (1971) Quadratic elongation: A quantitative measure of distortion in coordination polyhedral. *Science*, **172**, 567–570.

Schores, M.P., Nytko, E.A., Bartlett, B.M. and Nocera, D. G. (2005) Structurally perfect $S = ½$ kagomé antiferromagnet. *Journal of the American Chemical Society*, **127**, 13462–13463.

Sciberras, M.J., Leverett, P., Williams, P.A., Hibbs, D.E., Downes, P.J., Welch, M.D. and Kampf, A.R. (2013) Paratacamite-(Ni), $Cu_3(Ni,Cu)Cl_2(OH)_6$, a new mineral from Western Australia. *Australian Journal of Mineralogy*, **17**, 39–44.

Shannon, R.D. (1976) Revised effective ionic radii and systematic studies of interatomic distances in halides and chalcogenides. *Acta Crystallographica*, **A32**, 751–767.

Sheldrick, G.M. (2008) A short history of SHELX. *Acta Crystallographica*, **A64**, 112–122.

Smith, G.F.H. (1906) Paratacamite, a new oxychloride of copper. *Mineralogical Magazine*, **14**, 170–177

Welch, M.D., Sciberras, M.J., Leverett, P., Williams, P.A, Schlüter, J. and Malcherek, T. (2014) A temperature-induced reversible transformation between paratacamite and herbertsmithite. *Physics and Chemistry of Minerals*, **41**, 33–48.

Wulferding, D., Lemmens, P., Scheib, P., Röder, J., Mendels, P., Chu, S., Han, T. and Lee, Y.S. (2010) Interplay of thermal and quantum spin fluctuations in the kagomé lattice compound herbertsmithite. *Physical Review B*, **52**, 144412.

https://doi.org/10.1180/minmag.2016.080.079 Published online by Cambridge University Press